Imaging of Osteochondritis Dissecans

Andrew M. Zbojniewicz, MD*, Tal Laor, MD

KEYWORDS

• Osteochondritis dissecans • Cartilage • Ossification variation
• Magnetic resonance imaging (MRI) • Radiography • Knee • Elbow • Ankle

KEY POINTS

- Osteochondritis dissecans (OCD) can affect both adults and children, however the imaging characteristics and significance of imaging findings can differ in the juvenile subset with open physes.
- Radiography and magnetic resonance imaging (MRI) are the primary modalities used to aid in diagnosis, to define a treatment plan, to monitor progress, to assess surgical intervention, and to identify postoperative complications.
- Newer imaging techniques under continuous development may improve the accuracy of MRI for diagnosis and staging of OCD, and eventually may help to predict the durability of tissue-engineered constructs and cartilage repair.

Osteochondritis dissecans (OCD) can affect both adults and children, but the juvenile subset that is present in patients with open physes may have a different clinical course and prognosis.[1–5] The appearance and significance of imaging findings has similarly been shown to be different in children compared with adults.[6,7]

Radiographs constitute the initial imaging evaluation of patients with OCD but also are used to evaluate for lesion healing. Magnetic resonance imaging (MRI) may be used to confirm diagnosis and to aid in treatment planning. MRI also is useful to monitor healing with conservative management or after surgical intervention, and to aid in identification of complications in patients with continued pain.

KNEE

Imaging Diagnosis of OCD

The American Academy of Orthopaedic Surgeons (AAOS) guidelines for diagnosis and treatment of OCD give a weak recommendation for the use of conventional radiographs in patients with knee symptoms and/or signs suggesting OCD, based on a lack of strong evidence to suggest their efficacy.[8] However, radiographs are

Disclosures: The authors have no disclosures.
Department of Radiology, Cincinnati Children's Hospital Medical Center, University of Cincinnati College of Medicine, 3333 Burnet Avenue, Cincinnati, OH 45229, USA
* Corresponding author.
E-mail address: andrew.zbojniewicz@cchmc.org

Clin Sports Med 33 (2014) 221–250
http://dx.doi.org/10.1016/j.csm.2013.12.002 **sportsmed.theclinics.com**
0278-5919/14/$ – see front matter

inexpensive and readily available and therefore remain the mainstay of both diagnosis and monitoring of patients with OCD. Despite their continued widespread use, radiographs are limited by the lack of visualization of unossified elements, the inability to assess for mechanical instability, and the use of ionizing radiation.

Radiographic examination of the knee in the setting of possible OCD typically includes anteroposterior (AP), lateral, tunnel, and Merchant or sunrise views. The tunnel view is typically obtained with a posterior-to-anterior (PA) beam direction and approximately 30° to 40° of knee flexion, allowing improved visualization of the posterior femoral condyles. The Merchant view is performed with the patient supine and the knee flexed approximately 30° to best depict the femoral trochlea and patellar articular surface. OCD of the knee most commonly involves the lateral aspect of the medial femoral condyle (69%), followed by the lateral femoral condyle (15%), the patella (5%), and the femoral trochlea (1%).[9] The characteristic appearance of an OCD lesion on radiographs consists of a well-circumscribed lucent defect in subchondral bone that may or may not contain internal bone density (**Figs. 1** and **2**). However, in young children, subchondral irregularity or lucencies of either or both femoral condyles may reflect normal development, often referred to as irregular ossification or developmental ossification variation.

Similar to their recommendation regarding the use of radiography for diagnosis, the AAOS clinical practice guideline summary for diagnosis and treatment of OCD gave a weak recommendation for the use of MRI to characterize a known OCD lesion previously diagnosed with radiographs or to aid with diagnosis of concomitant disorder.[8] This weak recommendation was chosen in part because, at the time the guidelines were developed, no study had addressed the additional value of the use of MRI in the setting of an OCD lesion diagnosed with radiography. In addition, they cited inconsistent correlation of the MRI appearance of lesion instability with arthroscopic findings. In current practice, MRI is frequently used to attempt differentiation of a

Fig. 1. Juvenile OCD. AP standing radiograph from an 11-year-old boy football player shows a poorly circumscribed lucency (*arrow*) in the lateral aspect of the medial femoral condyle.

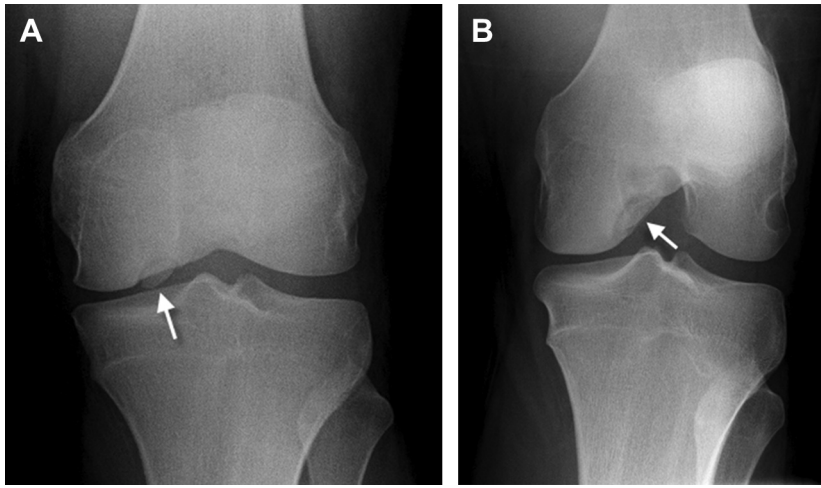

Fig. 2. Skeletally mature patient with OCD. (*A*) AP standing radiograph in a 17-year-old boy shows a well-circumscribed fragment of bone (*arrow*) within a lucent defect of the lateral aspect of the medial femoral condyle. (*B*) PA tunnel view, flipped to correspond with part (*A*), again shows the bone fragment (*arrow*).

developmental ossification variation from OCD, and following diagnosis of OCD to guide treatment by the assessment of whether a lesion is likely to be stable at the time of arthroscopy.

Developmental Ossification Variation and Juvenile Osteochondritis Dissecans of the Distal Femur

Sontag and Pyle[10] in 1941 followed by Caffey and colleagues[11] in 1958 found that distal femoral epiphyseal irregularities are common in children (aged 1–13 years) and resolve spontaneously, but can appear similar to radiographic findings in children diagnosed with OCD. Since that time, the differentiation of ossification variation from osteochondritis dissecans in children continues to be a difficult and controversial area of inquiry, with most attempts at delineation focused on MRI features.

An initial attempt to characterize ossification variations of the posterolateral femoral condyle on MRI was a report of 4 boys, aged 8 to 11 years, who despite osseous irregularity on MRI lacked clinical symptoms of the knee.[12] The investigators described these sites as islets of accessory ossification similar in signal intensity to the subchondral bone. The adjacent lucent zones identified on accompanying radiographs corresponded with areas similar in signal intensity to cartilage on MRI. Because earlier reports depicted juvenile OCD as abnormalities with hyperintense signal separating a lesion from the adjacent cartilage, the investigators concluded that, "MR imaging of osteochondritis dissecans may be clearly differentiated from those anomalies of ossification."

However, differentiation between the two diagnoses is not always well defined. Gebarski and Hernandez[13] suggested that accessory ossification centers and spiculations of the posterior inferocentral femoral condyles in children with substantial unossified epiphyseal cartilage, intact overlying cartilage, no associated edema, and bicondylar or bilateral location likely represent normal variants of ossification. A puzzle-piece configuration of the bone in the absence of edema is likely also a normal variation.[13] However, central intracondylar lesions with adjacent edema were findings associated with OCD.[13] The investigators concluded that normal ossification variation

can mimic early stage OCD, and this overlap in appearance might explain the great difference in outcomes associated with juvenile and adult forms of OCD.

Jans and colleagues[14] used these previously described criteria in their study population of 315 patients to divide children into a group with ossification variation and a group with juvenile OCD, in order to confirm previously described criteria and provide additional MRI features that might distinguish these two entities. They concluded that ossification variability did not occur in girls more than 10 years of age or in boys more than 13 years of age, was not seen if the child had 10% or less of residual unossified epiphyseal cartilage, and was found in the posterior third with occasional extension to the middle third of either femoral condyle. In contrast, OCD was rare in children with greater than 30% of residual unossified epiphyseal cartilage and was most frequently seen in the medial middle third of the femoral condyle. Extension into the intracondylar region was associated with OCD. It was also suggested that ossification variation extended deeper into the adjacent bone and showed no perilesional edema, whereas OCD lesions tended to be flatter and accompanied by adjacent bone marrow edema pattern.[14] Another study from the same group that did not exclude patients with general or anterior knee pain[15] found that the prevalence of variable femoral condylar ossification decreases with age, and is most common in boys. Peak age ranges for ossification variation was 2 to 12 years in boys and 2 to 10 years in girls. The same group in a third study concluded that ossification variations are not more common in children with OCD, and do not evolve into OCD lesions.[16]

In addition, it has been reported that juvenile OCD lesions consistently show disruption of the overlying normal thin hyperintense hemispherical secondary physis responsible for epiphyseal growth on water-weighted MRI sequences.[7] There may also be increased width of the unossified epiphyseal cartilage overlying OCD lesions compared with the adjacent, unaffected portions of condyle.[7] Whether the secondary physis is always continuous and the epiphyseal cartilage is similar in width to adjacent portions of the condyles in children with normal ossification variation is yet to be determined. **Table 1** summarizes many of the demographic and MRI features that have been reported with normal developmental ossification variation and with juvenile OCD that may be useful in their differentiation (**Figs. 3** and **4**).

Table 1
Features that may differentiate developmental ossification variation and juvenile OCD

Ossification Variation	Juvenile OCD
Demographics	
Girls <10 y of age, boys <13 y of age	Girls or boys >8 y of age
MRI Features	
No adjacent bone marrow edema	Adjacent bone marrow edema
Posterior third location ± extension to middle third; not anterior third	Usually middle third location
No intracondylar extension	—
Spiculation, puzzle pieces, accessory ossification centers	—
>10% residual cartilage	Rare with >30% residual cartilage
Deeper lesion (lesional angle <105°)	Flatter lesion (lesional angle >105°)
—	Disruption of secondary physis
—	Widened overlying unossified epiphyseal cartilage

Data from Refs.[7,13–16]

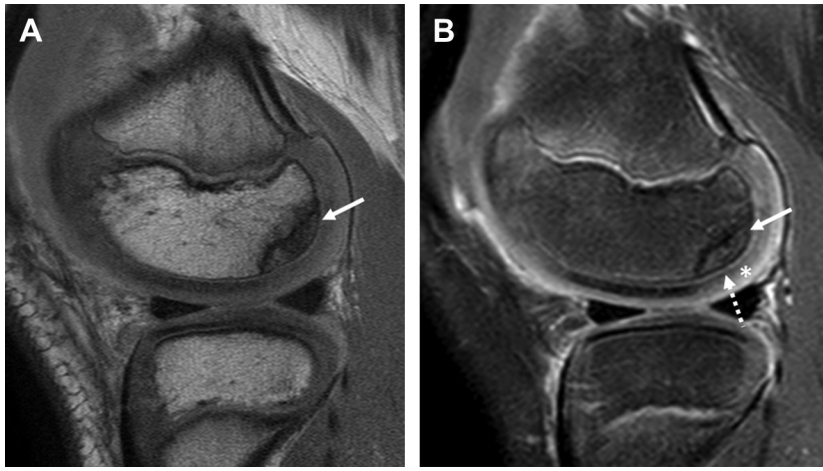

Fig. 3. Normal ossification variation. (*A*) Sagittal proton density–weighted image and (*B*) fat-suppressed T2-weighted image of the lateral femoral condyle from a 10-year-old boy show a puzzle-piece configuration (*arrows*) within the posterior third of the lateral femoral condyle. There is no adjacent bone marrow edema pattern, the secondary physis (*dashed arrow* in *B*) is intact, and the overlying unossified epiphyseal cartilage (*asterisk* in *B*) is not widened.

Fig. 4. Juvenile OCD. Sagittal fat-suppressed T2-weighted image of the medial femoral condyle from an 11-year-old boy shows osseous irregularity involving the middle and posterior thirds of the medial femoral condyle. There is adjacent bone marrow edema pattern (*arrow*) and the secondary physis (*dashed arrow*) becomes discontinuous at the lesion.

To date, although these studies have provided practitioners with useful guidelines to aid with differentiation of these two entities, the ability to define distinguishing features on MRI between normal ossification variation and juvenile OCD is limited by the retrospective nature of imaging reports, the absence of surgical and pathologic correlation, and the lack of longitudinal follow-up in children. However, correlation of clinical symptoms such as knee pain and swelling with the MRI appearance and patient demographics is often adequate to distinguish between these two entities.

Lesion Characteristics and Treatment Planning

Because of the inherent limitations of radiographic evaluation, which include underestimation of lesion size and inability to assess the integrity of overlying cartilage, MRI often is used to aid with formulation of a treatment plan.[9] Typical MRI sequences performed for the evaluation of OCD lesions include intermediate-weighted or T2-weighted fast spin echo (FSE) sequences in the sagittal or coronal plane with at least one plane fat suppressed, as well as a three-dimensional (3D) T1-weighted gradient recalled echo (GRE) sequence with fat suppression, typically in the sagittal plane.

There is abundant literature regarding the usefulness of MRI for staging OCD and the assessment of lesion stability.[6,17–25] De Smet and colleagues[17] in 1990 first reported one of the most widely recognized systems for the assessment of OCD lesion stability in the knee and ankle. The investigators identify 4 signs on T2-weighted images that were associated with instability of an OCD lesion, namely (1) hyperintense signal at the fragment-femur interface, (2) adjacent focal cystic areas, (3) displaced fragments within the joint, and (4) defects in articular cartilage. In 1996, the group went on to publish sensitivity and specificity values of these signs with slightly refined MRI criteria to include (1) either a well-defined or ill-defined line of hyperintense signal equal to that of fluid at the fragment-bone interface that measures 5 mm or more in length, (2) a discrete round focus of hyperintense signal deep to the OCD lesion measuring 5 mm or more, (3) a focal defect in the overlying articular cartilage that measures more than 5 mm in width, and (4) hyperintense signal equal to that of fluid that traverses both the articular cartilage and subchondral bone and extends into the lesion (**Figs. 5** and **6**).[18] Using these criteria, De Smet and colleagues[18] found a sensitivity of 97% and specificity of 100% for the detection of unstable OCD lesions. However, the investigators recognized that their patient cohort was small and therefore accurate conclusions regarding the value of imaging in the determination of lesion stability were limited. They suggested that, although a hyperintense T2 signal line present at the fragment-bone interface was sensitive, it may be less specific and may not necessarily indicate instability. In contrast, the investigators found that their other three signs were 100% specific for instability.

De Smet and colleagues[17,18] criteria did not distinguish between juvenile and adult patients with OCD, and the youngest patient in their cohort was 13 years old. To address this limitation, subsequent work by Kijowski and colleagues[6] determined that the aforementioned MRI criteria for lesion instability had a high specificity in adults, but not in children with OCD. This report used variations of the original criteria described in 1990, which included (1) linear rim of hyperintense signal surrounding the OCD on T2-weighted images with no mention of its need to be similar to signal intensity of joint fluid, (2) cysts surrounding the OCD lesion with no mention of cyst size, (3) hyperintense T2 signal fracture line that extends through the articular cartilage that overlies the OCD lesion, and (4) a fluid-filled osteochondral defect with no mention of size. These criteria were 100% sensitive and 100% specific for adult OCD, but although they were 100% sensitive for juvenile OCD, they were only 11% specific. The findings indicate that a hyperintense T2 signal rim or cystlike focus does not

Fig. 5. Unstable OCD in a skeletally mature 15-year-old girl. (*A*) Sagittal fat-suppressed T2-weighted image of the lateral aspect of the medial femoral condyle shows a focal defect in articular cartilage anteriorly (*arrow*) that measures more than 5 mm. An in situ fragment (*dashed arrow*) is seen within the posterior portion of the OCD. (*B*) The displaced osteochondral fragment (*arrow*) from the anterior portion of the lesion is seen in a more midline image. (*C*) There is a hyperintense T2 signal line 6 mm in length equal to the signal intensity of fluid at the lesion fragment-bone interface (*arrow*), which in addition to the incongruity of the articular surface indicates instability.

necessarily indicate instability in juvenile OCD (Fig. 7). However, if there was hyperintense rimlike T2 signal equal to that of joint fluid at the fragment-bone interface with a second deeper linear margin of hypointense T2 signal (Fig. 8), in addition to multiple sites of discontinuity of subchondral bone, these findings combined had both 100% sensitivity and 100% specificity for the determination of juvenile OCD instability. In addition, multiple cystlike foci or a single cystlike focus grater than 5 mm had sensitivities ranging from 25% to 38%, but specificity of 100% for the detection of instability (Fig. 9). A summary of imaging criteria used to suggest instability in both adult and juvenile OCD is provided in Table 2 .

Fig. 6. Unstable OCD. Coronal fat-suppressed T2-weighted image in a different skeletally immature 15-year-old girl shows a vertical hyperintense T2 signal line (*dashed arrow*) that traverses articular cartilage and courses toward the OCD fragment-bone interface. A more horizontal hyperintense T2 signal line (*arrow*) equal to fluid continues between the fragment and the underlying bone.

More recent studies[20,24] regarding the usefulness of MRI in the determination of juvenile OCD lesion stability corroborated these findings and revealed high sensitivity and low specificity for De Smet and colleagues'[17,18] original criteria.

However, these studies also did not use the refined criteria for juvenile OCD presented by Kijowski and colleagues[6] to assess for degree of improvement from the original criteria.

Lesion size measurement on MRI has been reported to be useful for treatment planning in children with a stable juvenile OCD lesion. Wall and colleagues[5] reported that lesion dimension normalized to femoral condyle size when plotted on a nomogram could be used to predict patient outcome. A recent study by Krause and colleagues[26] similarly suggested that age along with findings on MRI were able to help guide the choice between conservative and surgical treatment. A nomogram based on age, normalized lesion width, and size of cystlike foci on MRI was able to determine the healing potential of an OCD lesion at 6 months, and a cystlike focus smaller than 1.3 mm was associated with healing by 12 months.[26]

Posttreatment Imaging: Expected Findings and Complications

Following the diagnosis of an OCD lesion, a patient undergoes either conservative or surgical treatment. Conservative treatment of a stable juvenile OCD lesion may consist of activity modification, cast immobilization, or bracing and typically ranges in duration from 3 to 12 months.[9] Surgical treatment usually is used following failed conservative treatment or in the setting of an unstable OCD lesion, and entails either a primary repair or a salvage procedure.[9] Primary repair includes transarticular or retroarticular drilling and stabilization procedures, with or without bone grafting, or debridement of the lesion.[9] Salvage procedures include microfracture, osteochondral autograft or allograft, and autologous chondrocyte implantation (ACI).[9]

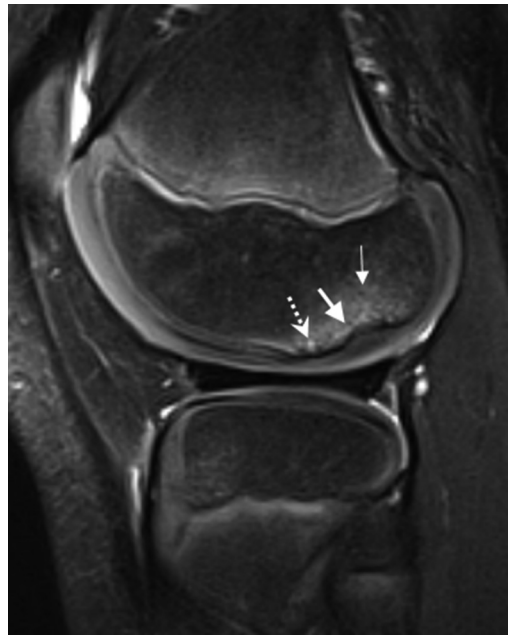

Fig. 7. Stable juvenile OCD. Sagittal fat-suppressed T2-weighted image from a 12-year-old shows a moderately hyperintense T2 signal rim (*thicker arrow*), but the hyperintense signal is not equal to fluid and does not contain an adjacent linear margin of hypointense T2 signal. There is a bone marrow edema pattern (*thinner arrow*), and a single small (<6 mm) cyst (*dashed arrow*) at the anterior margin of the lesion. The patient also has a discoid lateral meniscus. The OCD lesion was determined to be stable at surgery 1 month later.

Fig. 8. Unstable juvenile OCD. Coronal fat-suppressed T2-weighted image in a skeletally immature 17-year-old boy shows a rim of hyperintense T2 signal equal to fluid signal, with a deeper linear hypointense T2 signal margin (*solid arrow*), and multiple breaks in subchondral bone (*dashed arrows*).

Fig. 9. Large cystlike focus. Sagittal fat-suppressed T2-weighted image from a 14-year-old skeletally immature boy shows a single large 6-mm hyperintense signal cystlike focus (*arrow*) associated with a juvenile OCD lesion, which at arthroscopy was found to be unstable.

Table 2
MRI findings that suggest unstable OCD

Adult OCD[18] (T2-weighted Images)		Juvenile OCD[6] (T2-weighted Images)	
Well-defined or ill-defined hyperintense signal line equal to fluid signal at fragment-bone interface ≥5 mm	97% specificity, 100% sensitivity	Rimlike hyperintense signal equal to joint fluid signal + second deeper linear margin of low signal + multiple sites of discontinuity of subchondral bone	100% sensitive, 100% specific
Discrete round focus of high signal intensity ≥5 mm		Multiple cystlike foci or single cystlike focus >5 mm	Sensitivity 25%–38%, specificity 100%
Focal defect in articular cartilage >5 mm in width		—	—
Hyperintense signal line equal to fluid signal that traverses both articular cartilage and subchondral bone		—	—

Radiographs are the most frequent imaging modality used for monitoring children who undergo a conservative treatment plan. Assessment of healing on radiographs seems straightforward, but this can be deceiving. A variety of terms are used in the literature to describe radiographic signs of healing of an OCD lesion, and, as such, there are no standardized criteria. Terms such as reossification, disappearance of the radiolucent zone, resolution of the sclerotic rim, radiographic union of the lesion, resolution of the lesion, and resolution of the radiolucent demarcation around the lesion have all been used to indicate radiographic healing (**Fig. 10**).[27] A recent study by Parikh and colleagues[27] that did not use standardized criteria questions the reliability of the determination of healing based on conventional radiographs. Four reviewers evaluated radiographs from 39 children (mean age of 11.9 years) with OCD lesions of the knee who had been treated conservatively for 6 months. There was poor interrater reliability for the determination of healing of knee OCD lesions on

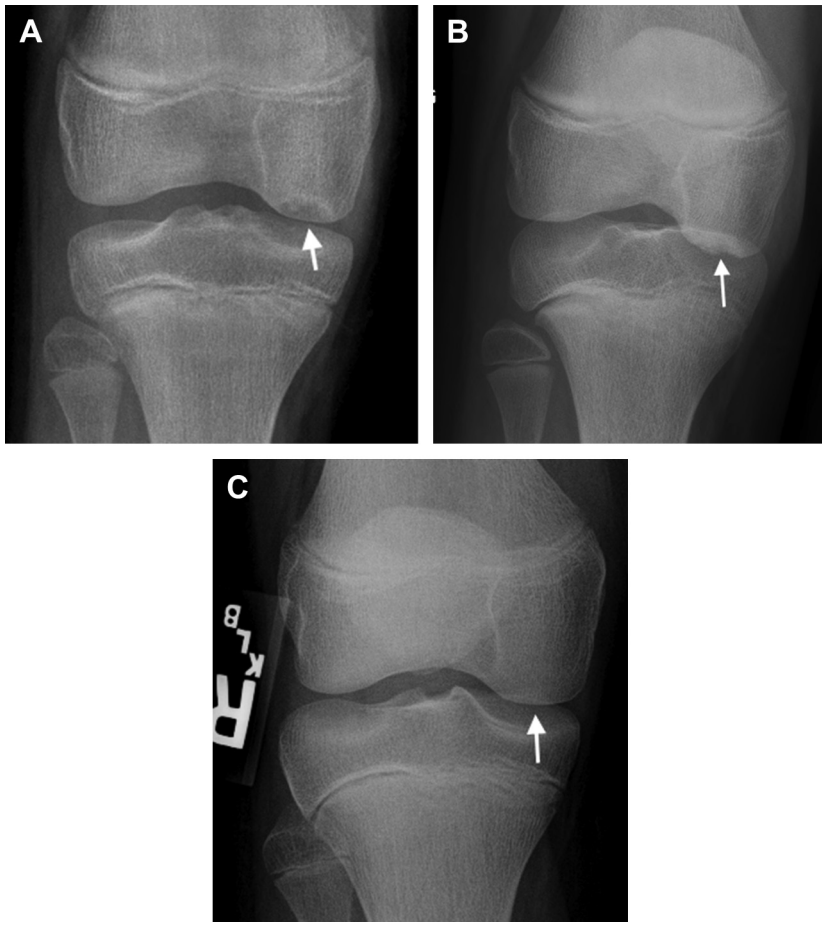

Fig. 10. Juvenile OCD lesion in an 11-year-old girl gymnast that healed over time with conservative management. (*A*) AP radiograph shows a well-circumscribed lucent defect (*arrow*) in the central medial femoral condyle. (*B*) Approximately 4 months later, there is increased sclerosis (*arrow*) within the OCD lesion. (*C*) Approximately 23 months after (*A*), the lesion appears healed (*arrow*).

radiographs, which suggests that standardized criteria are needed.[27] In addition, variation in image acquisition between patient visits can result in substantial difference in interpretation of healing over time. Tunnel views, in particular, can show different parts of the femoral condyles based on how steeply the radiography tube is angled and on the extent of knee flexion.

Radiographic findings that indicate previous surgical treatment commonly include transarticular screws (**Fig. 11**) and retroarticular drill tracks. Indicators of healing following surgery are similar to those recognized in the nonoperated knee, such as bone formation within the OCD defect and loss of the radiolucent zone of demarcation about the lesion. However, visualization of the condylar surface can be obstructed by screws.

MRI is often performed to assess healing in patients being treated conservatively, as well as in those who have undergone surgery. The recommended time interval for the assessment of healing on MRI in patients who undergo conservative management is variable depending on institutional protocol (time allowed for healing by conservative management) and surgeon preference. Although the recent study by Krause and colleagues[26] used MRI examinations exclusively at 6 months and 12 months to document healing, at our institution serial radiographs are used primarily for the first 6 months, with MRI reserved for cases with indeterminate healing, obtained usually at 6 months. MRI findings that suggest healing following conservative management include interval decrease or resolution in surrounding bone marrow edema pattern, decrease in lesion size, decrease or resolution of the hyperintense T2 signal rim or cystlike foci, and ingrowth of bone within the bed of the OCD lesion with bridging to the adjacent subchondral bone, best seen on non–fat-suppressed T1-weighted or GRE-weighted images.

Following surgical treatment of OCD, MRI allows a noninvasive assessment of repair tissue at both the articular surface and the bone-cartilage interface.[28] In order to evaluate repair cartilage in OCD lesions, MRI sequences similar to those used for the

Fig. 11. AP radiograph from a 9-year-old boy shows internal fixation of a juvenile OCD lesion of the medial femoral condyle by 3 headless compression screws.

diagnosis of OCD and those recommended by the International Cartilage Reparative Society for use in the evaluation of native cartilage, namely intermediate-weighted or T2-weighted FSE with or without fat suppression and T1-weighted GRE with fat suppression, should be used.[28] Non–fat-suppressed techniques result in greater signal to noise, which allows improved visualization of small abnormalities within cartilage. Therefore, protocols should include at least one plane without fat suppression to evaluate cartilage and one plane with fat suppression because of its increased sensitivity for marrow signal abnormalities. A T1-weighted sequence that is sensitive for marrow fat signal should also be performed in either the coronal or sagittal plane in order to assess for osseous integration. If MRI evaluation following a salvage procedure is desired, an initial examination at 3 to 6 months after surgery to assess the volume and integration of tissue is suggested,[28] followed by an additional examination at least 1 year after the procedure to assess incorporation and to identify postoperative complications.[28]

Retroarticular drilling and bone grafting does not result in the breach of articular cartilage. Therefore, lesional healing is expected to have a similar appearance to that observed with conservative management, namely the resolution of the bone marrow edema pattern and the hyperintense T2 signal rim or cystlike foci, as well as osseous ingrowth or incorporation of bone graft that fills the bed of the OCD lesion (**Fig. 12**). Surgical procedures that include microfracture and subchondral drilling frequently are used to allow multipotential stem cells in the surrounding marrow access into the OCD site and/or into areas of articular cartilage loss. The goal of these procedures is to promote healing of the OCD lesion or stimulate fibrocartilaginous tissue repair. Microfracture typically is used for cartilage defects smaller than 2 to 4 cm^2.[29]

Following microfracture, it can take up to 2 years for the defect to fill in completely with smooth and well-defined margins (**Fig. 13**).[28] In the first few months (usually 3–6 months) following the microfracture procedure, only thin and indistinct repair tissue may be present and should not be interpreted as treatment failure.[28] Because of a less organized matrix with increased water mobility, early reparative fibrocartilage may also show hyperintense signal on T2-weighted or intermediate-weighted FSE images compared with the hypointense signal intensity of adjacent native cartilage.[28] With maturation, this reparative tissue decreases in signal intensity and eventually may even become hypointense relative to native cartilage.[28,30] Although a subchondral bone marrow edema pattern may be present normally after surgery, it is expected to decrease over time.[28] A persistent bone marrow edema pattern in subchondral bone and lack of filling of the defect over time indicates treatment failure.[28] In contrast, overgrowth of subchondral bone is commonly seen (25%–49% of patients) and may not adversely affect clinical outcomes.[28,30] However, in select patients in whom bone overgrowth allows only a thin layer of reparative cartilage and poor lesional filling, there may be less favorable functional outcomes.[30] In addition, fissures are commonly seen at the junction of reparative fibrocartilage and native cartilage, but are not necessarily clinically relevant.[30]

Following a salvage procedure with osteochondral autograft, the defect should be filled by the graft. Eventual integration is heralded by trabecular incorporation between the plug and native bone, with uniform fat signal intensity on T1-weighted images (**Fig. 14**).[28,30] Small fissures between cartilage associated with the plug and the adjacent native cartilage often persist despite the graft otherwise appearing well incorporated.[28] These fissures have been shown at second-look arthroscopy to be filled with a fibrocartilaginous bond formed by organized scar tissue, and should not necessarily raise concern.[30] There should be a smooth transition between the surface of the native and the graft cartilage with complete restoration of the normal radius of curvature of

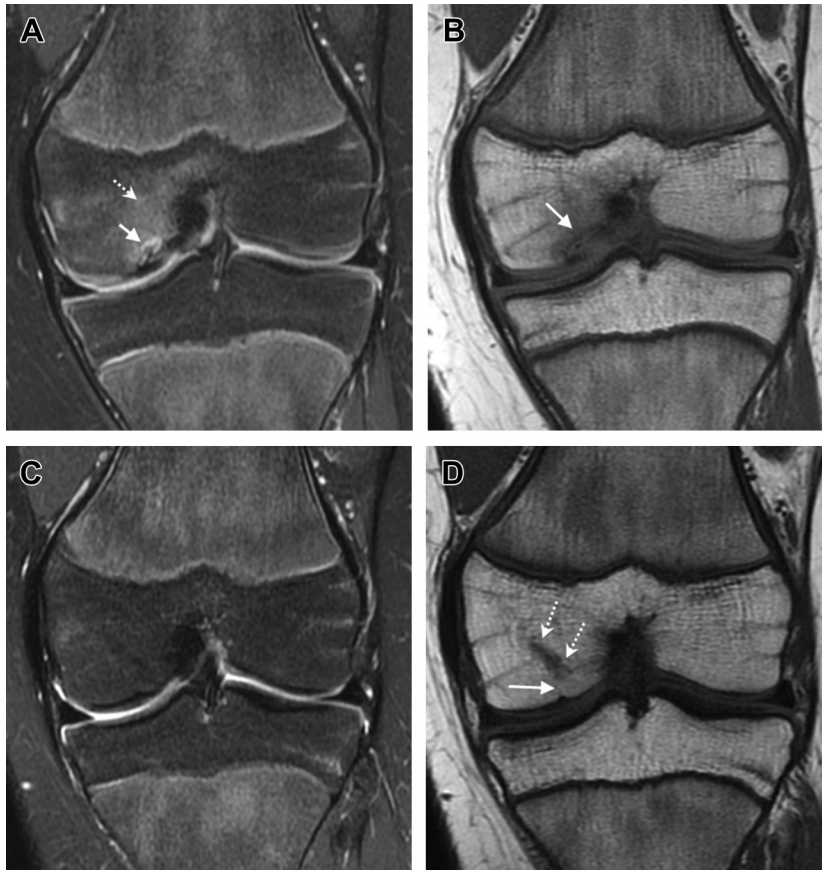

Fig. 12. Healed juvenile OCD lesion in a 14-year-old girl following retroarticular drilling and bone graft placement. (*A*) Coronal fat-suppressed T2-weighted image shows a hyperintense T2 signal rim (*arrow*) and bone marrow edema pattern (*dashed arrow*) within the medial femoral condyle. (*B*) The OCD lesion and adjacent bone marrow edema pattern are hypointense on this coronal T1-weighted image (*arrow*). (*C*) Approximately 14 months following surgery, a coronal fat-suppressed T2-weighted image shows resolution of the edema pattern and hyperintense signal rim. (*D*) Coronal T1-weighted image from the same time as (*C*) shows ingrowth of bone (*arrow*) at the site of the OCD lesion and adjacent retroarticular drill tracts (*dashed arrows*).

the condylar surface, which helps to maintain the biomechanical integrity of the plug.[28] Bone marrow edema pattern in and about the graft may be present in the first year following the procedure, but gradual reduction in this finding over time is expected.[28] Edema pattern in the graft has been reported in a small number of cases as late as 3 years following the procedure.[28] Joint effusion and synovial hypertrophy can persist for up to 2 years, and alone do not indicate graft failure.[28]

Lack of incorporation of an osteochondral autograft is suggested by fluid signal intensity at the interface between the graft and native bone, cystlike foci within subchondral bone, and a persistent bone marrow edema pattern (**Fig. 15**). Incongruity of the articular surface resulting in a loss of the normal radius of curvature can follow technical problems related to the initial press-fit placement of the graft or can be a more

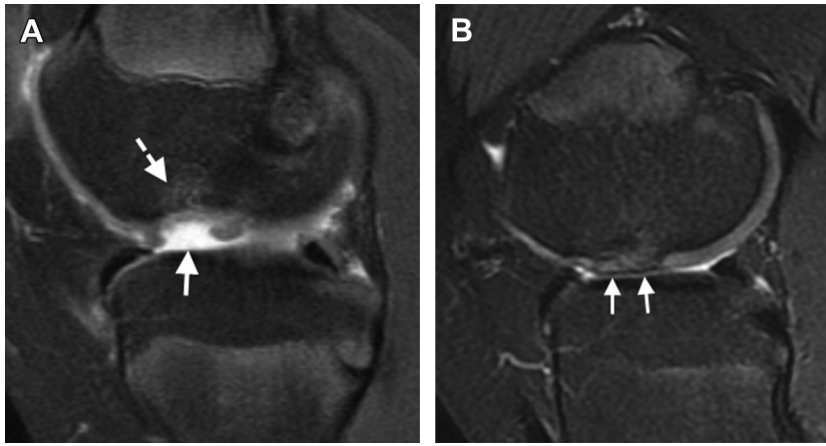

Fig. 13. Microfracture surgery. (*A*) Sagittal fat-suppressed T2-weighted image shows a large defect in articular cartilage (*arrow*) and subchondral bone marrow edema pattern (*dashed arrow*), consistent with an unstable juvenile OCD lesion. (*B*) Approximately 14 months following microfracture surgery, there is excellent fill of the OCD defect by reparative fibrocartilage, which has a similar signal intensity to native cartilage, and a smooth contour to the articular surface (*arrows*).

delayed manifestation of graft degradation of subsidence.[30] Another postsurgical complication is osteonecrosis of the plug, which is suggested on MRI by graft resorption and failure of osseous integration.[28]

Similar to osteochondral autografts, osteochondral allografts should be assessed for degree of fill of the osteochondral defect, integration of the graft, and a smooth transition between the surface of the native cartilage and the graft cartilage. Likewise, bone marrow edema pattern may be seen within the graft in the first 3 to 6 months following surgery, with a gradual decrease expected over time. Persistent bone marrow edema pattern 12 months after surgery, fluid signal intensity at the graft-host interface, or surface collapse may be indicators of graft rejection or lack of incorporation.[28] In addition, low signal intensity within the graft on all pulse sequences may be related to loss of bone viability and eventual implant failure.[30]

More recently, synthetic biphasic copolymer plugs have been used as a scaffold for bone and cartilage growth both to backfill donor sites in the setting of osteochondral autograft harvest or for primary cartilage repair.[30] Unlike autologous bone plugs, these are a scaffold and as such, presence of depression of the plug without restoration of the radius of curvature, resorption at the interface with native bone, and incomplete fill at less than 12 months all can be normal findings.[30] Complete incorporation can take more than 2 years, so a diagnosis of incomplete incorporation should be applied with caution.[30]

As opposed to microfracture, which is used for small lesions, ACI is often used for large defects (>2 cm^2) in articular cartilage. The classic procedure consists of a 2-stage operation; one to harvest healthy chondrocytes to be cultured in vitro for 3 to 5 weeks, and a second to implant the cultured chondrocytes with coverage by a periosteal flap that is secured in place with fibrin glue or sutures.[28] A second-generation procedure uses a bilayer collagen membrane instead of the periosteal flap.[28] A third-generation procedure, also known as matrix-induced autologous chondrocyte implantation (MACI) uses a collagen bilayer membrane as well, but with chondrocytes seeded into the membrane, allowing precise sizing of the membrane and fixation with fibrin glue alone. For deeper lesions (>8–10 mm), bone grafting is often

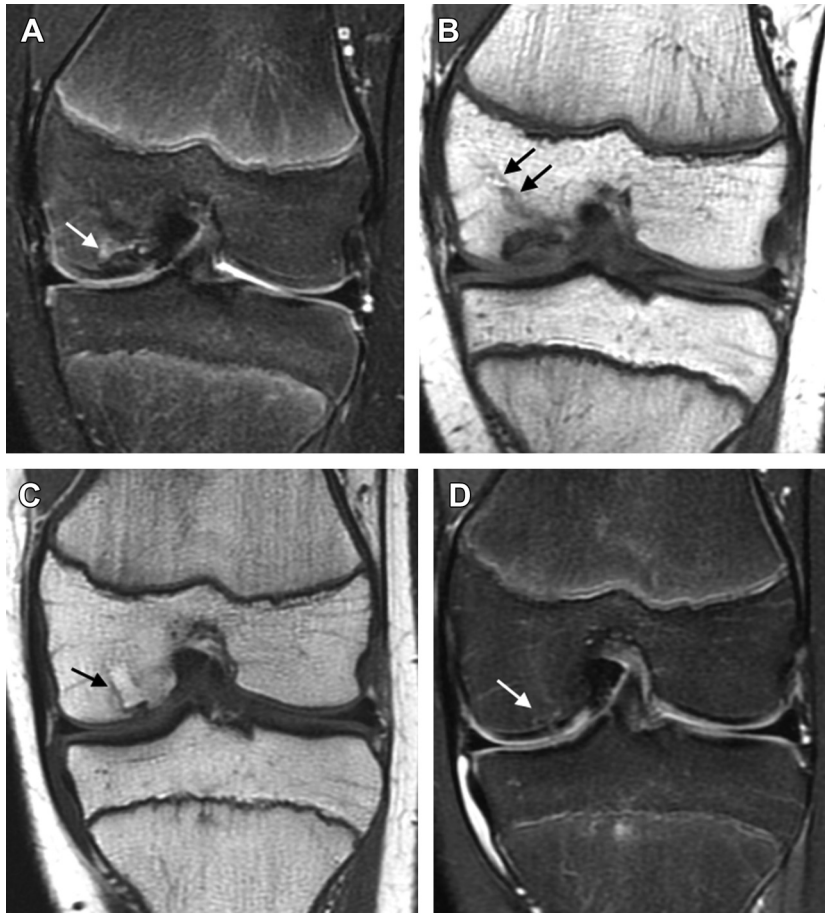

Fig. 14. Osteochondral autograft. (*A*) Coronal fat-suppressed T2-weighted image shows an OCD lesion (*arrow*) of the medial femoral condyle. (*B*) Coronal T1-weighted image shows tracks (*black arrows*) from retroarticular drilling and bone grafting performed approximately 1 year previously. (*C*) Coronal T1-weighted image obtained approximately 1 year after salvage procedure with placement of an osteochondral autograft shows excellent healing with incorporation of the osteochondral plug to the surrounding bone (*arrow*). (*D*) There is resolution of the hyperintense signal rim (*arrow*) on the coronal fat-suppressed T2-weighted image.

performed in conjunction with ACI. This is either performed as a staged operation with a separate surgery for bone grafting, or more recently with a "sandwich" technique. This technique consists of application of cancellous bone graft deep within the bed of the defect followed by placement of cultured chondrocytes "sandwiched" between periosteal or bilayer collagen membranes or by using two bilayer collagen membranes seeded with chondrocytes (MACI membranes).[28,31]

Three phases have been described in association with healing following ACI. The proliferative phase refers to the initial 6 weeks following surgery when the soft, primitive repair tissue begins to fill the site, although complete fill has been seen as early as 3 weeks after the procedure.[30] The transition phase involves expansion of the extracellular matrix and results in a gelatinlike consistency that occurs after 7 weeks to

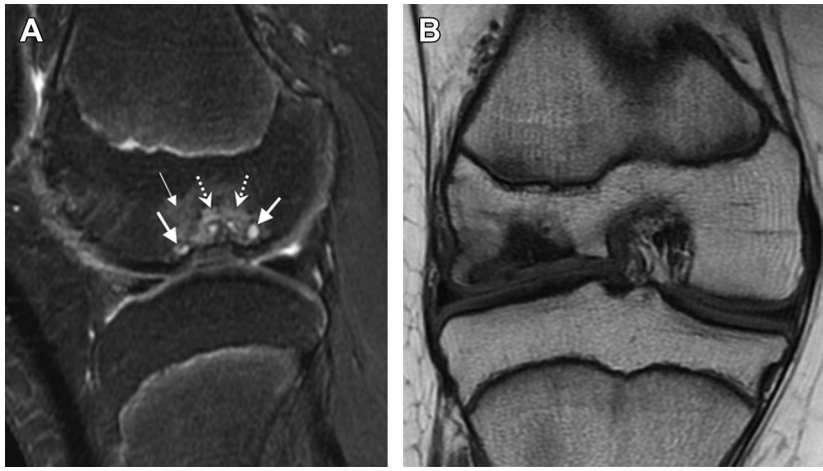

Fig. 15. Osteochondral autograft. (*A*) Sagittal fat-suppressed T2-weighted image shows hyperintense signal cystlike foci within subchondral bone (*thicker arrows*), and bone marrow edema pattern in the osteochondral plugs (*dashed arrows*) and in the surrounding bone (*thinner arrow*), which suggest lack of graft incorporation. (*B*) Coronal T1-weighted image shows hypointense signal at the OCD site, consistent with lack of osseous integration.

6 months, followed by the remodeling phase when hyalinelike repair cartilage is formed, at approximately 6 months to 3 years.[30] The MRI appearance reflects the histology, with early (less than 6 months after surgery) repair cartilage expected to be of hyperintense signal on T2-weighted or intermediate-weighted images relative to native cartilage, caused by the disorganization of the tissue architecture with resultant increased water content.[30] A gradual decrease in signal intensity is expected over time.[28,30] Filling of the defect by repair tissue can be described as flush, depressed, or proud, with a percent fill often characterized as either greater than or less than 50% of the depth of native cartilage.[28,30] Although ideally there should be complete filling of the defect with restoration of the normal radius of curvature of the articular surface, underfilling may not be clinically significant and requires further intervention in only approximately 2% of cases.[28,30] The interface of reparative cartilage with native cartilage is frequently not smooth, with small fissures less than 2 mm in width commonly seen.[30] In contrast, larger fissures are concerning for failed intergration.[30]

Two complications exclusive to ACI are cartilage delamination and cartilage overgrowth. Delamination typically occurs within 6 to 9 months of the procedure, is rare, and is seen in less than 5% of patients.[30] In situ delamination is indicated by fluid signal intensity between the cartilage repair tissue and the subchondral bone, whereas a displaced delaminated graft manifests as a fluid-filled defect at the repair site with a displaced intra-articular body.[30] Cartilage overgrowth typically occurs at 3 to 9 months after surgery and may consist of hypertrophy of the periosteal cover or thickening of the matrix.[30] On MRI, this is seen as extension of the periosteal cover or matrix beyond the normal contour of the articular cartilage or extension over the adjacent native cartilage.[30] Although frequently asymptomatic, patients can present with pain or a catching sensation that may require arthroscopic resection.[30] Persistence in subchondral bone marrow edema pattern over time and development of subchondral cysts also are concerning findings that may be seen with lack of integration.[30]

Transarticular screws or bioabsorbable pins often are used for fixation of an OCD lesion after primary repair, or occasionally as part of a salvage procedure. The severity

of metallic screw artifact on MRI depends on the type of hardware used, typically stainless steel or titanium. Stainless steel screws can obscure much, if not all, of the operative site (Fig. 16), whereas titanium screws result in minimal artifact (Fig. 17). Imaging parameters that can reduce MRI artifact from metal include the use of an increased bandwidth, small field of view, high-resolution matrix, thin slices, shorter echo time, and avoidance of fat-suppression techniques. The use of a short tau inversion recovery sequence also can reduce metal artifact. As an alternative, a new 3D FSE metal reduction sequence is now available for use in routine clinical practice that allows improved visualization of soft tissues around metal implants.

Bioabsorbable pins do not produce artifact on MRI. A study on the imaging appearance of polydioxanone biodegradable pins found that pins are linear in configuration and nearly always hypointense on T1-weighted images throughout the time course following surgery, whereas on T2-weighted images they tend to change gradually from hypointense to hyperintense signal over the first 12 months following placement, possibly because of hydrolyzed debris or fluid (see Fig. 17B).[28,32] Bone marrow edema pattern around the pins is seen in a minority of cases, generally decreasing over time.[32] In the study by Sirlin and colleagues,[32] 80% of the pins completely resorbed by 2 years.

Complications associated with bioabsorbable pins include failure of fixation or fracture, with subsequent displacement of all or part of the pin into the joint (Fig. 18). Transarticular screws can back out slightly, becoming proud relative to the articular surface, which may result in cartilage abnormalities of the adjacent tibia (see Fig. 17B). Radiographs are inadequate to define the relationship of screws to the articular surface, because articular cartilage and, in the case of juvenile OCD, unossified

Fig. 16. Artifact from stainless steel compression screws in the medial femoral condyle. Sagittal fat-suppressed T2-weighted image shows substantial metallic artifact that results in poor fat suppression and nonvisualization of the area surrounding the screws and the articular surface. There is also artifact from additional hardware in the proximal tibia.

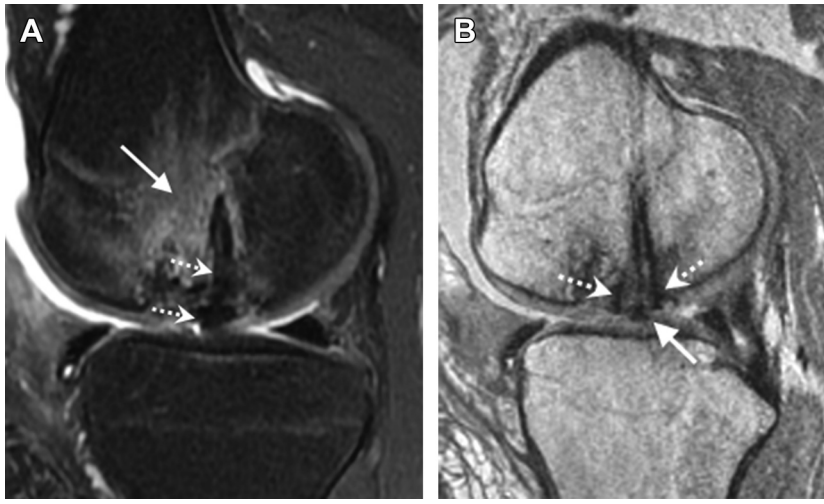

Fig. 17. Artifact from titanium compression screw in the lateral femoral condyle. (*A*) Sagittal fat-suppressed T2-weighted image shows only a small amount of artifact around the screw (*dashed arrows*). There is visualization of much of the OCD site as well adjacent bone marrow edema pattern (*solid arrow*). (*B*) Oblique sagittal 3D FSE proton density–weighted image in the same patient reformatted into the plane of the screw shows to better advantage the head of the screw (*arrow*). It has backed out slightly from the condyle and is in close approximation to the tibial articular surface. Bioabsorbable pins (*dashed arrows*) also are seen on either side of the compression screw.

epiphyseal cartilage cannot be visualized. However, MRI can be used to see the cartilage and evaluate the transarticular screws.

Future Developments in MRI of OCD

Recent developments in advanced imaging techniques may ultimately improve the accuracy of MRI in the diagnosis of OCD, may enable the refinement of treatment algorithms, and may further enhance the postsurgical assessment. One such imaging technique currently in clinical practice is a 3D FSE sequence capable of providing

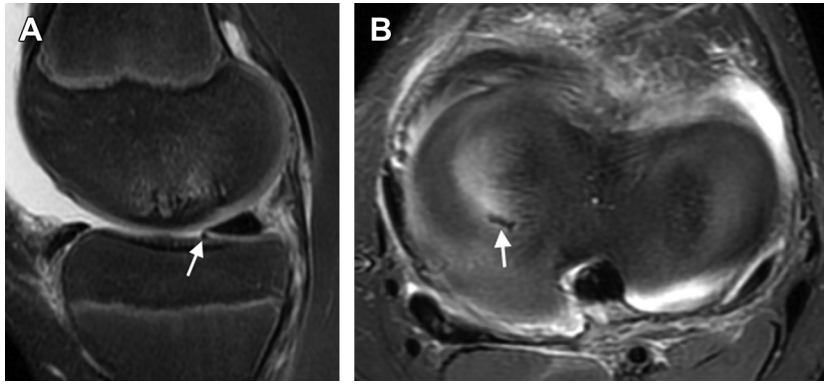

Fig. 18. Broken bioabsorbable pin. (*A*) Sagittal and (*B*) axial fat-suppressed T2-weighted images show a displaced screw fragment (*arrows*) lying inferior to the posterior horn of the medial meniscus.

high-resolution images with isotropic voxels. This technique allows thin sections (on the order of 1 mm or less) that can be reformatted into multiple planes with less volume averaging artifact, and already has been shown to increase the accuracy of MRI in the definition of abnormalities of articular cartilage in the knee.[33] This sequence may have a role in the improvement of accurate characterization of OCD lesions relative to arthroscopy and in the identification of complications following treatment (see Fig. 17B; Fig. 19).

Although most traditionally used MRI sequences subjectively evaluate the morphology of articular cartilage, newer techniques such as T2 mapping, T1ρ, and delayed gadolinium-enhanced MRI of cartilage (dGEMRIC) allow quantitative assessment of the composition of articular cartilage, as reflected by a tissue's T1 or T2 relaxation properties. These techniques give providers insight into the ultrastructure and biochemical properties of cartilage repair tissue and may allow objective measurement of treatment outcome, possibly even obviating biopsy, which traditionally has been the gold standard in the evaluation of success of repair (Fig. 20).[28,30,34] These quantitative sequences also have a potential role in the evaluation of unossified nonarticular cartilage in the setting of juvenile OCD. In addition, investigation is underway into the correlation between quantitative MRI assessment and material properties of cartilage with the hopes that imaging may eventually be able to predict the durability of tissue-engineered constructs and cartilage repair.[34]

ELBOW

OCD of the elbow most frequently involves the capitellum, although it also may involve the trochlea, radial head, and olecranon.[35] OCD needs to be differentiated from Panner disease, typically a self-limiting disorder of the capitellum that resolves with rest and little or no deformity. Panner disease is not associated with instability and as

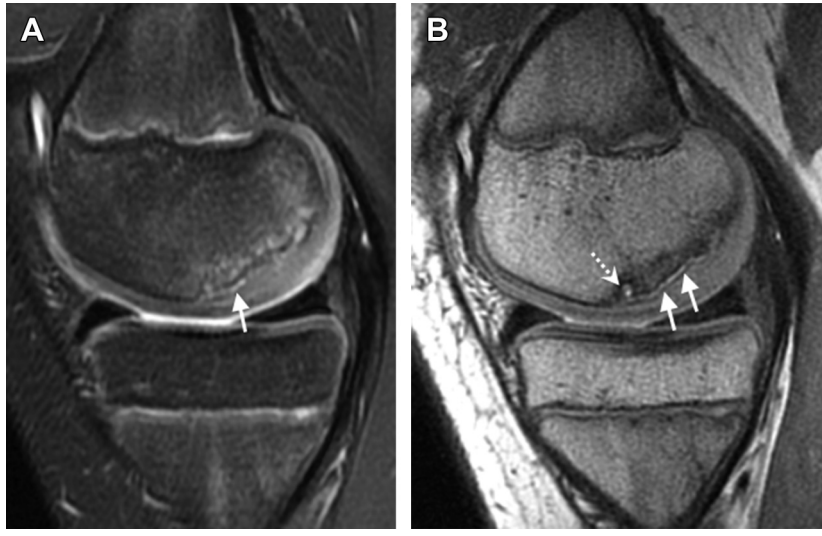

Fig. 19. (*A*) Sagittal fat-suppressed T2-weighted image shows a juvenile OCD lesion of the medial femoral condyle. There is a focal area of fluid signal intensity (*arrow*) at the interface between the OCD lesion and the subchondral bone. (*B*) Sagittal 3D FSE proton density–weighted image shows a well-defined hyperintense rim at the OCD-bone interface (*arrows*) and a small cystlike focus (*dashed arrow*) anteriorly.

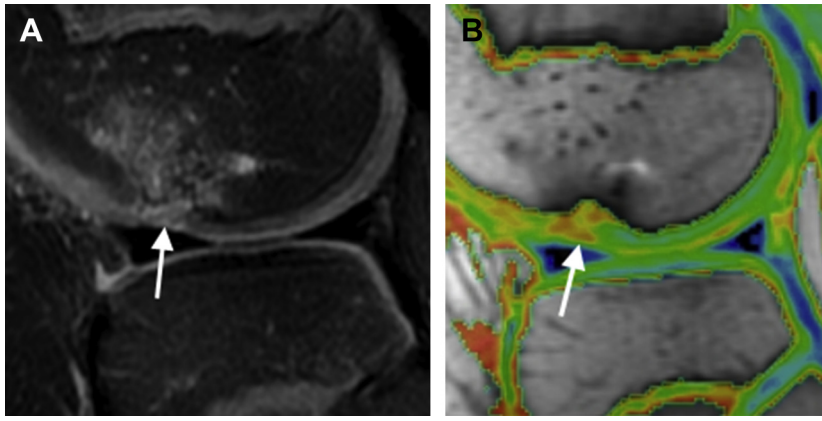

Fig. 20. T2 map of reparative cartilage. (*A*) Sagittal fat-suppressed T2-weighted image shows heterogeneous intermediate to hyperintense T2 signal material (*arrow*) within a site of microfracture performed 3 months earlier. This appearance suggests early reparative fibrocartilage. (*B*) Sagittal color-coded map of T2 relaxation time values shows abnormal red color (*arrow*) at the site of the reparative fibrocartilage, consistent with an abnormally long T2 relaxation time compared with the green color within the adjacent normal cartilage. The prolonged T2 relaxation time indicates disorganized tissue with greater mobility of water.

such only shows abnormal radiolucency, flattening or irregularity of the capitellum on radiographs, or hypointense T1 signal and possibly mild hyperintense T2 signal on MRI, but no loose bodies (**Fig. 21**). In contrast, OCD in the elbow has a limited capacity for healing with a potential for fragmentation and formation of loose intra-articular bodies, which occasionally result in degenerative joint disease. Panner disease is seen typically in young, growing children less than 10 years of age, whereas OCD usually presents in the young adolescent athlete with average age range of onset of 12 to 17 years.[35]

Radiographic examination in a patient suspected of having OCD of the elbow consists of an AP view in full extension and a lateral view with 90° of flexion. Radiographic findings of capitellar OCD include rarefaction/radiolucency, flattening of the articular surface, fragmentation with demarcating sclerosis, and intra-articular bodies.[35] Radial head enlargement and osteophyte production infrequently are seen as late findings.[35]

Staging was reportedly developed by Minami and colleagues, in which a grade 1 lesion was described as a translucent or cystic shadow of the middle or lateral aspect of the capitellum, a grade 2 lesion showed a split line or clear zone of demarcation between the lesion and subchondral bone, and a grade 3 lesion was characterized by an intra-articular loose body.[35] However, recent studies have questioned the sensitivity of radiographs for diagnosis and characterization of capitellar OCD.[36,37] Kijowski and De Smet[37] found that, even with a retrospective review, radiographs alone had limited sensitivity in detecting OCD of the capitellum and associated intra-articular loose bodies. In this study, which included 15 patients, only 66% of OCD were identified on initial interpretation of radiographs and only 57% of intra-articular bodies were seen. Because of the limitations in the standard AP and lateral elbow evaluation for diagnosis of OCD, it has been suggested by other investigators that adding an AP view with the elbow in 45° of flexion may improve radiographic detection of capitellar OCD.[35]

Because of limitations in radiographic evaluation, MRI frequently is performed in patients suspected of having capitellar OCD but who have normal radiographs, or in

Fig. 21. Panner disease. (*A*) AP radiograph of an 8-year-old boy with elbow pain shows irregularity (*arrow*) of the capitellar ossification center. (*B*) Sagittal T1-weighted image shows hypointense signal (*arrow*) at the site of irregularity. (*C*) Fat-suppressed T2-weighted image shows mildly hyperintense signal (*arrow*) at the same location.

patients diagnosed with OCD who require further evaluation. Similar to MRI indications for OCD of the knee, the primary role of MRI for evaluating a known OCD of the elbow is to detect an unstable lesion, which will alter treatment planning and prognosis.

Kijowski and DeSmet[38] found that the criteria defined for OCD of the knee by DeSmet and colleagues[17,18] also can be applied to the assessment of lesion stability at the elbow (**Fig. 22**).

Jans and colleagues,[39] who used the conditions described by Kijowski and colleagues[6] for the assessment of instability of juvenile OCD in the knee, found that these criteria, when used together, were 100% sensitive for the assessment of instability of OCD lesions at the elbow in patients with a mean age of 14 years of age, although each

Fig. 22. Unstable capitellar OCD. (*A*) Frontal radiograph shows the characteristic focal lucency in the capitellum (*arrows*) indicating an OCD lesion. (*B*) Sagittal fat-suppressed T2-weighted image shows rimlike hyperintense signal similar to fluid at the fragment-bone interface (*arrow*), which suggests instability. (*C*) Twenty-one months later, the patient presents with limitation of elbow extension. A fat-suppressed T2-weighted image now shows a displaced fragment (*arrow*) in the posterior aspect of the elbow joint.

criterion was not sensitive when used alone. They also identified correctly the 3 arthroscopically proven stable lesions in their study population using these criteria, although specificity was not commented on. In contrast, a study by Iwasaki and colleagues[40] performed in overhead athletes also with a mean age of 14 years (but 5 patients between 16 and 20 years of age and 1 patient >20 years of age) found that De Smet and colleagues'[17,18] original criteria had only an 89% sensitivity and 44% specificity for the prediction of fragment instability. MRI performed poorly in the determination of lesion stability compared with surgery as the gold standard, although their study

had recognized limitations. These limitations included a small number of patients with preoperative MRI examinations indicating stability and a selection bias in that only patients with surgical correlation were used for the study, thus selecting for a group of patients that had either a more advanced stage of OCD or long-standing symptoms not responsive to conservative treatment.[40]

In addition, clinicians should not confuse an OCD lesion of the capitellum, which typically is in the anterolateral aspect of the capitellum, with the normal anatomic variant referred to as a pseudodefect, which is located more posteriorly between the smooth articular surface of the posterior-inferior capitellum and the adjacent lateral epicondyle (**Fig. 23**).[38]

ANKLE

At the ankle, the broader term osteochondral lesion (OCL) is often used instead of OCD because of the recognition that many of these lesions are the direct result of trauma. The term OCD is reserved for a distinct subset of OCLs that may be associated with a genetic, endocrine, or metabolic abnormality and does not necessarily require a history of antecedent trauma.[41,42] Similar to the elbow, a classification system developed by Berndt and Harty[43] in 1959 based on radiography was used originally to help stage patients with OCLs of the talus. Stage 1 lesions were characterized by focal subchondral trabecular compression; stage 2 by a partially detached fragment; stage 3 by a completely detached, in situ fragment; and stage 4 by a detached

Fig. 23. Pseudodefect of the capitellum. Sagittal 3D fat-suppressed T1-weighted gradient echo image shows irregularity (*arrow*) at the junction of the posteroinferior capitellum and adjacent lateral epicondyle, the characteristic site and appearance of a pseudodefect.

and displaced fragment. Similar to other radiographically based classification systems, its strength lies in its simplicity; however, like other radiographically based systems, subsequent studies have shown that it is not very sensitive, with up to 50% of OCLs not detected on conventional radiographs.[42] Numerous staging systems were subsequently proposed between 1986 and 2003, which include a modification to Berndt and Harty's[43] original system, as well as systems based on arthroscopy, computed tomography (CT), and most commonly MRI.[19,44–48]

OCLs of the talus were classically described to occur in the anterolateral and posteromedial talar dome; however, recent studies that used MRI have shown that most lesions are located medially and centrally, followed by a lateral and central location.[49,50] Although most commonly seen in the talar dome, OCLs may involve many other sites about the ankle, which include the talar head, tibial plafond, cuboid, navicular, subtalar joint, and various metatarsal heads.[41]

On CT, subchondral cystlike foci, as well as detachment, fragmentation, and displacement of bone fragments, are features that suggest instability (**Fig. 24**). Despite the usefulness of CT to provide additional characterization of an OCL, MRI is the preferred modality because of its ability to visualize abnormality in adjacent bone marrow and overlying cartilage, which results in improved sensitivity for early stage OCLs.[41] MRI is often ordered in the clinical setting of a conservatively treated ankle sprain with prolonged pain refractory to treatment and normal radiographs to assess for a radiographically occult OCL.[41]

Early OCLs may manifest simply as a focal area of bone marrow edema pattern, sometimes flame shaped, on T2-weighted images at one side of a joint.[41] However, MRI may overestimate the severity of injury within the bone, and a bone marrow edema pattern does not necessarily indicate acuity of injury. Bone marrow edema pattern can be seen acutely in the setting of a bone bruise as well as chronically in the setting of reactive marrow changes related to long-standing instability or osteoarthritis, among other causes.[42]

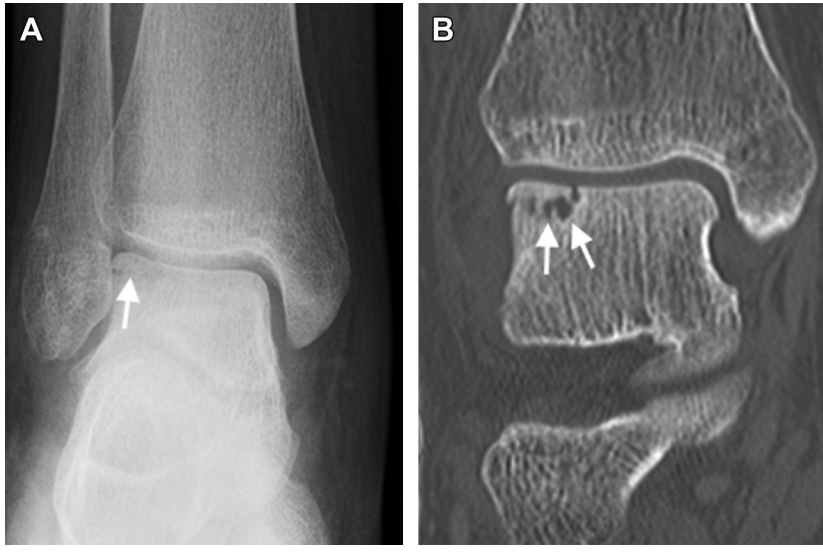

Fig. 24. Unstable talar osteochondral lesion. (*A*) AP radiograph shows an osteochondral lesion (*arrow*) of the lateral talar dome. (*B*) Coronal CT reformation better reveals cystlike foci (*arrows*) at the base of the OCL in this surgically proven unstable lesion.

Fig. 25. Stable talar osteochondral lesion. Coronal fat-suppressed T2-weighted image shows subchondral marrow edema pattern (*arrow*) of the lateral talar dome, indicating a low-grade OCL.

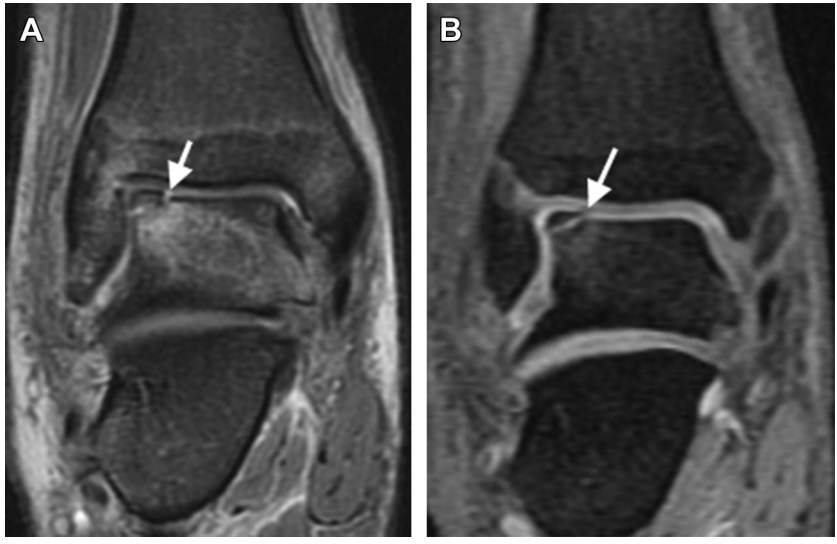

Fig. 26. Unstable talar osteochondral lesion. (*A*) Coronal fat-suppressed T2-weighted image shows a fissure containing fluid signal intensity (*arrow*) at the medial margin of the OCL, with discontinuity of the subchondral bone. (*B*) The same fissure (*arrow*) but with disruption of the hyperintense signal articular cartilage on a fat-suppressed 3D T1-weighted GRE sequence.

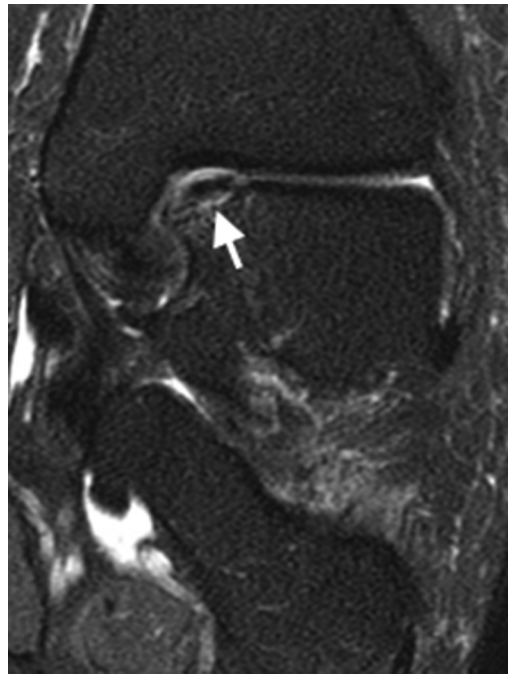

Fig. 27. Unstable osteochondral lesion. Coronal fat-suppressed T2-weighted image shows a hyperintense T2 signal rim (*arrow*) similar to fluid signal intensity at the fragment-bone interface.

Accurate description and assessment of OCL stability is a useful goal for MRI evaluation. De Smet and colleagues[17] original criteria for lesions of the knee are applicable to lesions of the ankle, and may be used to provide imaging support for the diagnosis of instability. Similar to the original Berndt and Harty[43] classification system, bone marrow edema pattern indicates subchondral compression or bone bruise, but without other abnormality it suggests a mild or early stage OCL (**Fig. 25**). In a similar way, articular cartilage damage either characterized by hyperintense signal on T2-weighted images or surface fibrillation typically is present in an earlier stage OCL, whereas deeper fissures that extend to bone, cystlike foci, or a hyperintense rim on T2-weighted images that indicate a loose, but nondisplaced fragment suggest a later stage OCL (**Figs. 26** and **27**). Other features that may suggest instability include extensive bone marrow edema pattern out of proportion to any recent trauma, or interval collapse of the articular surface since the initial injury.[41]

SUMMARY

Various imaging modalities can be used as important adjuncts to a physical examination and surgical therapy in the treatment of patients with OCD. Both radiographs and MRI can be used to aid in diagnosis, to define a treatment plan, to monitor progress, to assess surgical intervention, and to identify postoperative complications. In addition to well-established imaging techniques, newer MRI sequences may hold promise for objective evaluation of tissue composition and integrity.

REFERENCES

1. Clanton TO, DeLee JC. Osteochondritis dissecans. History, pathophysiology and current treatment concepts. Clin Orthop Relat Res 1982;(167):50–64.
2. Glancy GL. Juvenile osteochondritis dissecans. Am J Knee Surg 1999;12(2):120–4.
3. Hefti F, Beguiristain J, Krauspe R, et al. Osteochondritis dissecans: a multicenter study of the European Pediatric Orthopedic Society. J Pediatr Orthop B 1999;8(4):231–45.
4. Pill SG, Ganley TJ, Milam RA, et al. Role of magnetic resonance imaging and clinical criteria in predicting successful nonoperative treatment of osteochondritis dissecans in children. J Pediatr Orthop 2003;23(1):102–8.
5. Wall EJ, Vourazeris J, Myer GD, et al. The healing potential of stable juvenile osteochondritis dissecans knee lesions. J Bone Joint Surg Am 2008;90(12):2655–64. http://dx.doi.org/10.2106/JBJS.G.01103.
6. Kijowski R, Blankenbaker DG, Shinki K, et al. Juvenile versus adult osteochondritis dissecans of the knee: appropriate MR imaging criteria for instability. Radiology 2008;248(2):571–8. http://dx.doi.org/10.1148/radiol.2482071234.
7. Laor T, Zbojniewicz AM, Eismann EA, et al. Juvenile osteochondritis dissecans: is it a growth disturbance of the secondary physis of the epiphysis? AJR Am J Roentgenol 2012;199(5):1121–8. http://dx.doi.org/10.2214/AJR.11.8085.
8. Chambers HG, Shea KG, Carey JL. AAOS clinical practice guideline: diagnosis and treatment of osteochondritis dissecans. J Am Acad Orthop Surg 2011;19(5):307–9.
9. Moktassi A, Popkin CA, White LM, et al. Imaging of osteochondritis dissecans. Orthop Clin North Am 2012;43(2):201–11. http://dx.doi.org/10.1016/j.ocl.2012.01.001, v–vi.
10. Sontag LW, Pyle SI. Variations in the calcification pattern in epiphyses. AJR Am J Roentgenol 1941;45:50–4.
11. Caffey J, Madell SH, Royer C, et al. Ossification of the distal femoral epiphysis. J Bone Joint Surg Am 1958;40-A(3):647–54 passim.
12. Nawata K, Teshima R, Morio Y, et al. Anomalies of ossification in the posterolateral femoral condyle: assessment by MRI. Pediatr Radiol 1999;29(10):781–4.
13. Gebarski K, Hernandez RJ. Stage-I osteochondritis dissecans versus normal variants of ossification in the knee in children. Pediatr Radiol 2005;35(9):880–6. http://dx.doi.org/10.1007/s00247-005-1507-6.
14. Jans LB, Jaremko JL, Ditchfield M, et al. MRI differentiates femoral condylar ossification evolution from osteochondritis dissecans. A new sign. Eur Radiol 2011;21(6):1170–9. http://dx.doi.org/10.1007/s00330-011-2058-x.
15. Jans LB, Jaremko JL, Ditchfield M, et al. Evolution of femoral condylar ossification at MR imaging: frequency and patient age distribution. Radiology 2011;258(3):880–8. http://dx.doi.org/10.1148/radiol.10101103.
16. Jans L, Jaremko J, Ditchfield M, et al. Ossification variants of the femoral condyles are not associated with osteochondritis dissecans. Eur J Radiol 2012;81(11):3384–9. http://dx.doi.org/10.1016/j.ejrad.2012.01.009.
17. De Smet AA, Fisher DR, Graf BK, et al. Osteochondritis dissecans of the knee: value of MR imaging in determining lesion stability and the presence of articular cartilage defects. AJR Am J Roentgenol 1990;155(3):549–53. http://dx.doi.org/10.2214/ajr.155.3.2117355.
18. De Smet AA, Ilahi OA, Graf BK. Reassessment of the MR criteria for stability of osteochondritis dissecans in the knee and ankle. Skeletal Radiol 1996;25(2):159–63.

19. Dipaola JD, Nelson DW, Colville MR. Characterizing osteochondral lesions by magnetic resonance imaging. Arthroscopy 1991;7(1):101–4.
20. Heywood CS, Benke MT, Brindle K, et al. Correlation of magnetic resonance imaging to arthroscopic findings of stability in juvenile osteochondritis dissecans. Arthroscopy 2011;27(2):194–9. http://dx.doi.org/10.1016/j.arthro.2010.07.009.
21. Mesgarzadeh M, Sapega AA, Bonakdarpour A, et al. Osteochondritis dissecans: analysis of mechanical stability with radiography, scintigraphy, and MR imaging. Radiology 1987;165(3):775–80. http://dx.doi.org/10.1148/radiology.165.3.3685359.
22. Nelson DW, DiPaola J, Colville M, et al. Osteochondritis dissecans of the talus and knee: prospective comparison of MR and arthroscopic classifications. J Comput Assist Tomogr 1990;14(5):804–8.
23. O'Connor MA, Palaniappan M, Khan N, et al. Osteochondritis dissecans of the knee in children. A comparison of MRI and arthroscopic findings. J Bone Joint Surg Br 2002;84(2):258–62.
24. Samora WP, Chevillet J, Adler B, et al. Juvenile osteochondritis dissecans of the knee: predictors of lesion stability. J Pediatr Orthop 2012;32(1):1–4. http://dx.doi.org/10.1097/BPO.0b013e31823d8312.
25. Yoshida S, Ikata T, Takai H, et al. Osteochondritis dissecans of the femoral condyle in the growth stage. Clin Orthop Relat Res 1998;(346):162–70.
26. Krause M, Hapfelmeier A, Moller M, et al. Healing predictors of stable juvenile osteochondritis dissecans knee lesions after 6 and 12 months of nonoperative treatment. Am J Sports Med 2013;41(10):2384–91. http://dx.doi.org/10.1177/0363546513496049.
27. Parikh SN, Allen M, Wall EJ, et al. The reliability to determine "healing" in osteochondritis dissecans from radiographic assessment. J Pediatr Orthop 2012;32(6):e35–9. http://dx.doi.org/10.1097/BPO.0b013e31825fa80f.
28. Choi YS, Potter HG, Chun TJ. MR imaging of cartilage repair in the knee and ankle. Radiographics 2008;28(4):1043–59. http://dx.doi.org/10.1148/rg.284075111.
29. Behery O, Siston RA, Harris JD, et al. Treatment of cartilage defects of the knee: expanding on the existing algorithm. Clin J Sport Med 2013. http://dx.doi.org/10.1097/JSM.0000000000000004.
30. Hayter C, Potter H. Magnetic resonance imaging of cartilage repair techniques. J Knee Surg 2011;24(4):225–40.
31. Bartlett W, Gooding CR, Carrington RWJ, et al. Autologous chondrocyte implantation at the knee using a bilayer collagen membrane with bone graft. J Bone Joint Surg (Br) 2005;87-B:330–2.
32. Sirlin CB, Boutin RD, Brossmann J, et al. Polydioxanone biodegradable pins in the knee: MR imaging. AJR Am J Roentgenol 2001;176(1):83–90. http://dx.doi.org/10.2214/ajr.176.1.1760083.
33. Crema MD, Roemer FW, Marra MD, et al. Articular cartilage in the knee: current MR imaging techniques and applications in clinical practice and research. Radiographics 2011;31(1):37–61. http://dx.doi.org/10.1148/rg.311105084.
34. Potter HG, Black BR, Chong le R. New techniques in articular cartilage imaging. Clin Sports Med 2009;28(1):77–94. http://dx.doi.org/10.1016/j.csm.2008.08.004.
35. Baker CL 3rd, Romeo AA, Baker CL Jr. Osteochondritis dissecans of the capitellum. Am J Sports Med 2010;38(9):1917–28. http://dx.doi.org/10.1177/0363546509354969.
36. Janarv PM, Hesser U, Hirsch G. Osteochondral lesions in the radiocapitellar joint in the skeletally immature: radiographic, MRI, and arthroscopic findings in 13 consecutive cases. J Pediatr Orthop 1997;17(3):311–4.

37. Kijowski R, De Smet AA. Radiography of the elbow for evaluation of patients with osteochondritis dissecans of the capitellum. Skeletal Radiol 2005;34(5):266–71. http://dx.doi.org/10.1007/s00256-005-0899-6.
38. Kijowski R, De Smet AA. MRI findings of osteochondritis dissecans of the capitellum with surgical correlation. AJR Am J Roentgenol 2005;185(6):1453–9. http://dx.doi.org/10.2214/AJR.04.1570.
39. Jans LB, Ditchfield M, Anna G, et al. MR imaging findings and MR criteria for instability in osteochondritis dissecans of the elbow in children. Eur J Radiol 2012;81(6):1306–10. http://dx.doi.org/10.1016/j.ejrad.2011.01.007.
40. Iwasaki N, Kamishima T, Kato H, et al. A retrospective evaluation of magnetic resonance imaging effectiveness on capitellar osteochondritis dissecans among overhead athletes. Am J Sports Med 2012;40(3):624–30. http://dx.doi.org/10.1177/0363546511429258.
41. Naran KN, Zoga AC. Osteochondral lesions about the ankle. Radiol Clin North Am 2008;46(6):995–1002. http://dx.doi.org/10.1016/j.rcl.2008.10.001, v.
42. O'Loughlin PF, Heyworth BE, Kennedy JG. Current concepts in the diagnosis and treatment of osteochondral lesions of the ankle. Am J Sports Med 2010;38(2):392–404. http://dx.doi.org/10.1177/0363546509336336.
43. Berndt A, Harty M. Transchondral fractures (osteochondritis dissecans) of the talus. J Bone Joint Surg Am 1959;41-A:988–1020.
44. Ferkel RD, Zanotti RM, Komenda GA, et al. Arthroscopic treatment of chronic osteochondral lesions of the talus: long-term results. Am J Sports Med 2008;36(9):1750–62. http://dx.doi.org/10.1177/0363546508316773.
45. Hepple S, Winson IG, Glew D. Osteochondral lesions of the talus: a revised classification. Foot Ankle Int 1999;20(12):789–93.
46. Mintz DN, Tashjian GS, Connell DA, et al. Osteochondral lesions of the talus: a new magnetic resonance grading system with arthroscopic correlation. Arthroscopy 2003;19(4):353–9. http://dx.doi.org/10.1053/jars.2003.50041.
47. Pritsch M, Horoshovski H, Farine I. Arthroscopic treatment of osteochondral lesions of the talus. J Bone Joint Surg Am 1986;68(6):862–5.
48. Taranow WS, Bisignani GA, Towers JD, et al. Retrograde drilling of osteochondral lesions of the medial talar dome. Foot Ankle Int 1999;20(8):474–80.
49. Elias I, Zoga AC, Morrison WB, et al. Osteochondral lesions of the talus: localization and morphologic data from 424 patients using a novel anatomical grid scheme. Foot Ankle Int 2007;28(2):154–61. http://dx.doi.org/10.3113/FAI.2007.0154.
50. Hembree WC, Wittstein JR, Vinson EN, et al. Magnetic resonance imaging features of osteochondral lesions of the talus. Foot Ankle Int 2012;33(7):591–7. http://dx.doi.org/10.3113/FAI.2012.0001.